Shear response estimate for squat reinforced concrete walls via a single panel model

Leonardo M. Massone[*] and Marco A. Ulloa[a]

Department of Civil Engineering, University of Chile, Blanco Encalada 2002, Santiago, Chile

Abstract. Squat reinforced concrete walls require enough shear strength in order to promote flexural yielding, which creates the need for designers of an accurate method for strength prediction. In many cases, especially for existing buildings, strength estimates might be insufficient when more accurate analyses are needed, such as pushover analysis. In this case, estimates of load versus displacement are required for building modeling. A model is developed that predicts the shear load versus shear deformation of squat reinforced concrete walls by means of a panel formulation. In order to provide a simple, design-oriented tool, the formulation considers the wall as a single element, which presents an average strain and stress field for the entire wall. Simple material constitutive laws for concrete and steel are used. The developed models can be divided into two categories: (i) rotating-angle and (ii) fixed-angle models. In the first case, the principal stress/strain direction rotates for each drift increment. This situation is addressed by prescribing the average normal strain of the panel. The formation of a crack, which can be interpreted as a fixed principal strain direction is imposed on the second formulation via calibration of the principal stress/strain direction obtained from the rotating-angle model at a cracking stage. Two alternatives are selected for the cracking point: fcr and 0.5fcr (post-peak). In terms of shear capacity, the model results are compared with an experimental database indicating that the fixed-angle models yield good results. The overall response (load-displacement) is also reasonable well predicted for specimens with diagonal compression failure.

Keywords: squat wall; panel model; strength; backbone; reinforced concrete; shear

1. Introduction

Structural walls are frequently used to improve building stiffness and strength. Squat walls, which present low aspect ratio (less than 2) are common in nuclear plants, low-rise buildings, building facades and parking lots. In RC structures two regions can be distinguished, the B- and D-regions (Schlaich *et al*. 1987). B-regions are those remote from the area of load application (or reaction) or discontinuities, where the Bernoulli hypothesis for bending theory is reasonable. D-regions are those that are close to the points of load application or discontinuities, where the stress flow is distorted. In the case of squat walls, low slenderness and a combination of axial and lateral loads results in highly distorted stress flows. This situation challenges many models, especially if

---

[*]Corresponding author, Ph. D., Associate Professor, E-mail: lmassone@ing.uchile.cl
[a]Former civil engineering student

they are design-oriented capable of predicting the shear strength or providing more information such as the load versus displacement response, which might be useful for pushover analysis.

Several models have been used to idealize the response of squat walls. Finite element formulation with a reasonable RC model has shown good correlation with experimental results (Palermo and Vecchio 2002; Mo *et al*. 2008). Even simpler formulations based on fibers that are modeled with panel behavior provide good response (Massone *et al*. 2009; Massone 2010). However, such approaches are still far from being massively used by designers, given the need of specific non-linear analysis software (usually non-commercial). Other models, while having a physical approach to the wall shear response, are yet still simple. These models can be divided in two groups: (1) strut and tie models and (2) panel models. Strut and tie models are a common formulation for D-regions, but most of them are intended to predict shear strength of structures providing compression concrete truss elements (strut) in the direction of compression stresses and reinforcing steel in the direction of tensile forces. The model by Hwang *et al*. (2001), which has shown good shear strength prediction belong to this category. The model uses three main struts, one along the main diagonal of the walls and other two struts going through higher and lower directions, respectively. The strength estimate is determined by means of equilibrium in the node, after applying constitutive material laws for concrete and steel. The shear strength is known once the concrete compressive strength is reached. The model, similar to others within this category, can only predict the shear strength. Panel models, in the other hand, assume uniform stress/strain fields within the entire wall section, which allows obtaining the shear force versus shear displacement response. The work by Hsu and Mo (1985) presents one of the first attempts to predict the shear response of walls with this approach. In their publication compatibility is established for the entire wall, constitutive material loads are defined for concrete and steel, and equilibrium is determined in the longitudinal (vertical) direction, which results in a nonlinear equation that requires solution for each displacement step. In order to solve the equilibrium equation the transverse normal strain (expansion) is considered equal to zero. This approach results in a principal stress/strain direction that rotates with the increment of lateral displacement (rotating-angle approach). Other similar proposed models have varied the assumption in the strain field, instead of assuming zero expansion, the location of the principal strain (and stress for most models) direction is set as the main diagonal geometric direction of the wall section (Gupta and Rangan 1998). This is also limited by either zero transverse strain (large constrain) or zero transverse stress (free edge). In this case, the principal stress/strain direction is fixed (fixed-angle approach). Examples of rotating-angle and fixed-angle approach models can be found in Hsu and Mo (2010). A current research has shown that the cracking pattern might not be consistent with the direction of the main diagonal geometric direction (Kaseem and Elsheikh 2010). The work by Kaseem and Elsheikh instead of using a prescribed transverse stress or strain (usually zero) provided a calibrated expression for the principal strain/stress direction based on a best-fit of shear strength estimate for a database of wall tests. Good predictions, in this case, are sensitive to the selected database and extrapolation of the use of the calibrated principal stress/strain direction might not be adequate.

This publication deals with the development and validation of a panel model for squat walls capable of predicting the shear strength as well as the shear load versus shear displacement. The model uses a similar methodology to the one developed by Kaseem and Elsheikh, but determines the principal stress/strain direction differently. Two approaches are considered: (1) rotating-angle (crack) and (2) fixed-angle (crack) models, which are based on calibrated normal (vertical and horizontal) average strains in walls.
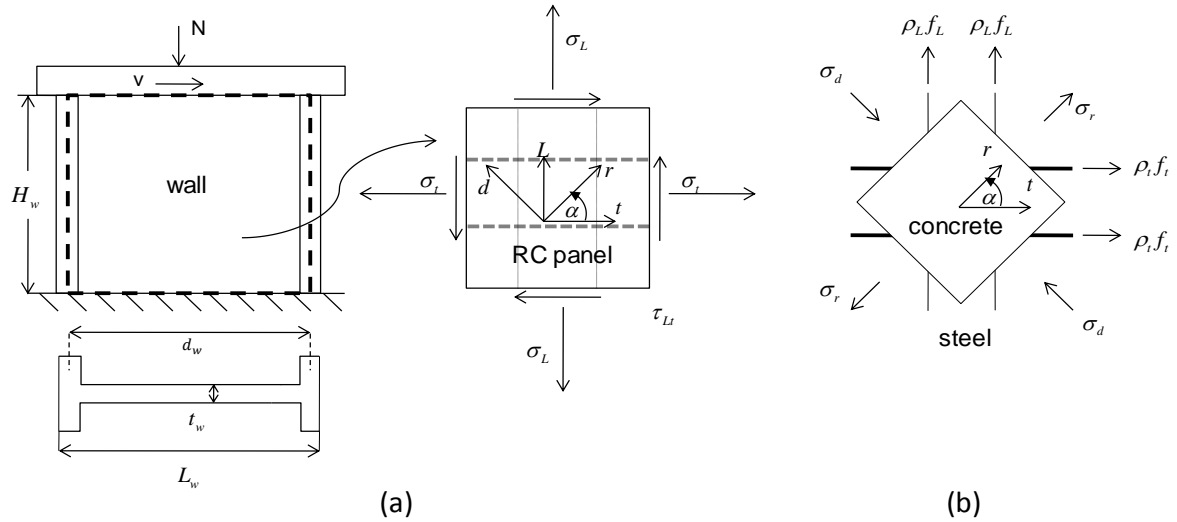
Fig. 1 Wall configuration: (a) geometry and resultant stresses, (b) concrete and steel stresses (after Kaseem and Elsheikh 2010)

2. Model formulation

Similarly to previous panel model formulations (Hsu and Mo 1985; Gupta and Rangan 1998; Kaseem and Elsheikh 2010), the material model for reinforced concrete is based on the idea of the modified compression field theory (MCFT) (Vecchio and Collins 1986). The MCFT establishes the panel concrete response in the two principal directions based on uniaxial material constitutive laws, including softening of concrete in compression due to cracking in the orthogonal direction (other principal direction). Steel response is incorporated assuming perfect adherence between concrete and steel.

2.1 Geometrical model

Once a diagonal crack develops in the wall element, the web steel reinforcing bars are subject to tensile forces and concrete usually sustain forces in compression in one principal direction and tensile forces in an orthogonal direction. Fig. 1a shows the horizontal and vertical reinforcements which are oriented in directions L and t, forming the L-t coordinate system. The principal direction of concrete in compression goes along direction d, which is inclined at an angle α with respect to the longitudinal direction of the vertical reinforcement (Fig. 1b). The direction perpendicular to d is called r (principal tensile direction).

2.2 Equilibrium and compatibility

Assuming that web steel reinforcement is subjected to stresses along its longitudinal direction (no dowel action) and reinforcement is placed in two orthogonal directions (L, t); equilibrium equations governing the system in the L-t coordinate are represented as follows,

$$\sigma_L = \sigma_d cos^2\alpha + \sigma_r sin^2\alpha + \rho_L f_L = \frac{N}{A} \qquad (1)$$

$$\sigma_t = \sigma_d sin^2\alpha + \sigma_r cos^2\alpha + \rho_t f_t \qquad (2)$$

$$\tau_{Lt} = (-\sigma_d + \sigma_r)cos\alpha \; sin\alpha \qquad (3)$$

where f_L and f_t are the average reinforcement stress in directions L and t, respectively, ρ_L and ρ_t are the web steel reinforcing ratio in the same respective directions, σ_L and σ_t are the average normal stress in the reinforced concrete panel in the respective directions, τ_{Lt} is the concrete shear stress in the plane L-t, and finally, σ_d and σ_r are the principal concrete stresses in the principal directions d and r (Fig. 1b). In Eq. (1), N is the applied axial load and A is the area between flange (or enlarged wall boundary) element centroids (Fig. 1a).

Assuming that the stress distribution in the wall web is uniform, the shear resultant force can be expressed as follows,

$$V = \tau_{Lt} t_w d_w \qquad (4)$$

where t_w is the wall web thickness and d_w is the horizontal distance between flange element centroid (Fig. 1a). In rectangular walls, it is assumed that $d_w = 0.8L_w$, where L_w is the wall length. Compatibility is established for the entire panel section, assuming that stress (concrete) and strain field principal directions coincide, yielding,

$$\varepsilon_L = \varepsilon_d cos^2\alpha + \varepsilon_r sin^2\alpha \qquad (5)$$

$$\varepsilon_t = \varepsilon_d sin^2\alpha + \varepsilon_r cos^2\alpha \qquad (6)$$

$$\gamma_{Lt} = 2(\varepsilon_r - \varepsilon_d)cos\alpha \; sin\alpha \qquad (7)$$

where $\varepsilon_L, \varepsilon_t, \varepsilon_d$ and ε_r are the normal strain values consistent with directions L, t, d and r, respectively, and γ_{Lt} is the shear strain in the L-t plane. Assuming that the wall top lateral displacement is governed by the shear strain, the lateral displacement is determined as,

$$\Delta = \gamma_{Lt} H_w \qquad (8)$$

where H_w is the wall height (Fig. 1a).

2.3 Material constitutive laws

2.3.1 Concrete

Selected material properties are identical as incorporated by Kaseem and Elsheikh (2010). Concrete constitutive law in compression is proposed by Zhang and Hsu (1998), which considers the degradation of concrete compressive capacity due to tensile strain (cracking) in the orthogonal direction. Assuming that direction d corresponds to the compressive principal direction, the compressive (σ_d, negative for compression) response is described as follows,

$$\sigma_d = -\zeta f'_c \left[2\left(\frac{-\varepsilon_d}{\zeta\varepsilon_0}\right) - \left(\frac{-\varepsilon_d}{\zeta\varepsilon_0}\right)^2 \right], \ \ if \ \varepsilon_d \leq \zeta\varepsilon_0 \tag{9}$$

$$\sigma_d = -\zeta f'_c \left[1 - \left(\frac{\frac{-\varepsilon_d}{\zeta\varepsilon_0}-1}{\frac{2}{\zeta}-1}\right)^2 \right], \ \ if \ \varepsilon_d > \zeta\varepsilon_0 \tag{10}$$

$$\zeta = \frac{5.8}{\sqrt{f'_c}} \frac{1}{\sqrt{1+400\varepsilon_r}} \leq \frac{0.9}{\sqrt{1+400\varepsilon_r}} \tag{11}$$

where f'_c is the concrete compressive strength, ε_0 is the compressive strain consistent with f'_c (solid line, Fig. 2a), ζ is the reduction factor due to cracking (Fig. 2a) that causes softening in the compressive direction. As seen in Fig. 2a, ζ reduces the peak concrete strength and also the strain at peak stress (dotted line). Assuming that the r direction corresponds to the principal tensile direction, concrete in tension (σ_r, positive for tension) is modeled according to Gupta and Rangan (1998) proposition as follows,

$$\sigma_r = E_c\varepsilon_r, \ \ if \ 0 \leq \varepsilon_r \leq \varepsilon_{ct} \tag{12}$$

$$\sigma_r = f'_{ct} \frac{(\varepsilon_{ut}-\varepsilon_r)}{(\varepsilon_{ut}-\varepsilon_{ct})}, \ \ if \ \varepsilon_{ct} < \varepsilon_r \leq \varepsilon_{ut} \tag{13}$$

$$\sigma_r = 0, \ \ if \ \varepsilon_{ut} < \varepsilon_r \tag{14}$$

where $f'_{ct} = 0.4\sqrt{f'_c(MPa)}$ is the tensile concrete strength with $\varepsilon_{ct} = f'_{ct}/E_c$ and $E_c = 4700\sqrt{f'_c(MPa)}$. Ultimate tensile strain, ε_{ut}, is set as 0.002 which coincides with steel yielding for most cases (Fig. 2b).

2.3.2 Reinforcing steel

The uniaxial model for reinforcing steel uses an elasto-plastic stress (f_s) versus strain (ε_s) response (Fig. 2c), defined as,

$$f_s = E_s\varepsilon_s, \ \ if \ \varepsilon_s < \varepsilon_y \tag{15}$$

$$f_s = f_y, \ \ if \ \varepsilon_s \geq \varepsilon_y \tag{16}$$

where E_s is the steel reinforcement elastic modulus, f_y is the yield stress of steel. Subscript "s" is replaced by "t" or "L" for transverse or longitudinal reinforcement, respectively.

2.4 Strain field

As mentioned earlier, different assumptions have been used by previous researchers that allow estimation of the principal stress/strain angle (α). Some of them have being based on zero stress or strain values in the horizontal normal direction arguing that either the wall side faces are free of forces (usually not too short walls) or the wall cannot expand horizontally due to support (pedestal, beam) constrain (extremely short walls), respectively. Imposition of one of these two assumptions allows determination of the principal strain/stress direction. In other cases, the principal direction is simply forced in the direction of the wall geometric main diagonal.
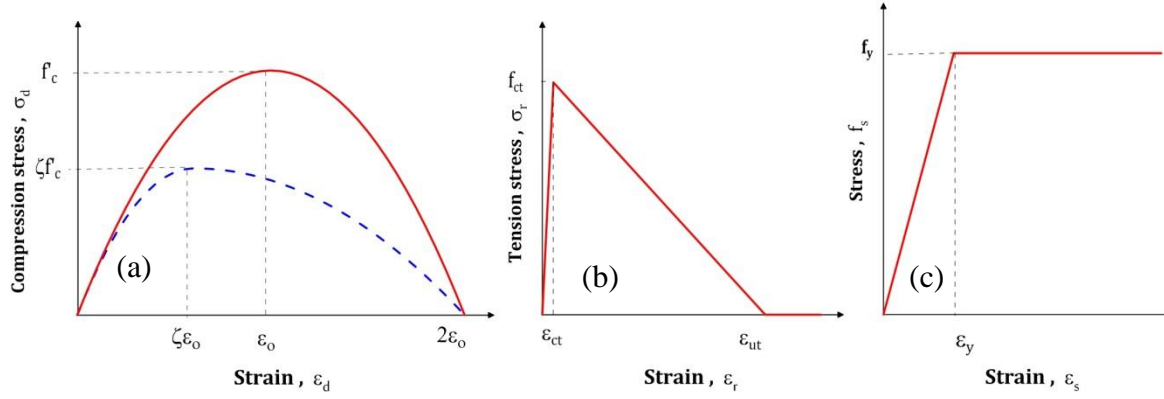
Fig. 2 Material constitutive laws: (a) concrete in compression, (b) concrete in tension, and (c) steel.

A previous research calibrated expressions for the average wall expansion (average transverse strain) along the wall height, which was used to provide an input for a model that offers a coupled response between shear and flexure for a displacement-based element (Massone 2010). The calibrated expressions are based on a two-dimensional finite element formulation with consistent material and panel model. Thus, the model uses the same principles defined by the MCFT (Vecchio and Collins 1986). Calibration of wall expansion was performed over a database of analytical results for a broad range of geometric parameters, as well as, material properties, vertical and horizontal web steel ratio, level of axial load and boundary condition. Validation of the analytical expression with experimental data indicates good correlation. According to the study (Massone 2010), the expressions for walls with fixed-end condition (double curvature) and free-end condition (cantilever) are defined as follows,

Double curvature

$$\varepsilon_{t,max} = 0.0033(100\rho_t + 0.25)^{-0.53}\left(\frac{H_w}{L_w} + 0.5\right)^{0.47}\left(\frac{100N}{f'_c t_w L_w} + 5\right)^{0.25}(100\delta)^{1.4} \quad (17)$$

$$\frac{\varepsilon_t(y)}{\varepsilon_{t,max}} = sin^{0.75}\left(\frac{y}{H_w}\pi\right) \quad (18)$$

Cantilever

$$\varepsilon_{t,max} = 0.0055(100\rho_t + 0.25)^{-0.44}(100\delta)^{1.4} \quad (19)$$

$$\frac{\varepsilon_t(y)}{\varepsilon_{t,max}} = \begin{cases} sin^{0.75}\left(\frac{y}{0.76H_w}\pi\right) & if \ 0 \leq y \leq 0.38H_w \\ sin^{0.75}\left(\frac{y+0.24H_w}{1.24H_w}\pi\right) & if \ 0.38H_w < y \leq H_w \end{cases} \quad (20)$$

where $\delta = \Delta/H_w$ is the wall lateral top drift, and y is the vertical location (measured from wall base). The maximum values of average expansion ($\varepsilon_{t,max}$) are located at $0.5H_w$ for double-curvature walls and at $0.38H_w$ for cantilever walls (Eq. 17 and 19), and transverse strains vary along the height according to Eq. 18 and 20. As for the implementation in this work an average strain field is required, therefore the expression is integrated over the height yielding an average (over the height) value of $\varepsilon_t = 0.69\varepsilon_{t,max}$.

For the vertical average normal strain (ε_L) for walls a similar procedure was performed (Villar

2010), yielding the following expressions,

Double curvature

$$\varepsilon_L = 0.0094(100\rho_t + 0.25)^{-0.17}\left(\frac{H_w}{L_w} + 0.5\right)^{-0.16}\left(\frac{100N}{f'_c t_w L_w} + 5\right)^{-0.35}(100\delta) + \varepsilon_N \qquad (21)$$

Cantilever

$$\varepsilon_L = 0.0089(100\rho_t + 0.25)^{-0.25}\left(\frac{H_w}{L_w} + 0.5\right)^{-0.37}\left(\frac{100N}{f'_c t_w L_w} + 5\right)^{-0.34}(100\delta)^{0.93} + \varepsilon_N \quad (22)$$

where $\varepsilon_N = -\frac{N}{t_w L_w E_c}$ is an estimate of the elastic (E_c, concrete elastic modulus) normal strain due to the applied axial load N.

2.5 Rotating-Angle (RA) model

The previous expressions for the wall transverse (ε_t) and longitudinal (ε_L) average normal strain together with the drift level (assumed as the shear strain, γ_{Lt}), provides the full components of the strain field. The principal strain direction is determined by combining Eq. 5, 6 and 7, yielding $\alpha = tan^{-1}\left(-\frac{(\varepsilon_t - \varepsilon_L)}{\gamma_{Lt}} + \sqrt{\left(\frac{\varepsilon_t - \varepsilon_L}{\gamma_{Lt}}\right)^2 + 1}\right)$, which changes (rotates) with the variation of strain values. The main characteristic of this model is that the algorithm is non-iterative. This is because the strain field ($\varepsilon_t, \varepsilon_L$ and $\gamma_{Lt} = \delta$) is known for the wall panel for every drift level, which makes possible obtaining the stress field (σ_t, σ_L and τ_{Lt}) by using the constitutive material laws, leading to an estimate of the shear resultant by equilibrium (Eq. 4). In this way, the equilibrium equation in the vertical direction is not necessarily satisfied (Eq. 1).

Fig. 3 shows the variation of the principal strain direction (α) predicted by the model for specimen T-5 (Orakcal *et al*. 2009) with axial load (N=0.1f'_cA_g) and specimen G-8 (Galletly 1952) without axial load. Similar results are obtained with other specimens distinguished by the axial load. The wall with axial load (Fig. 3a) shows an angle that increases with drift until a point where
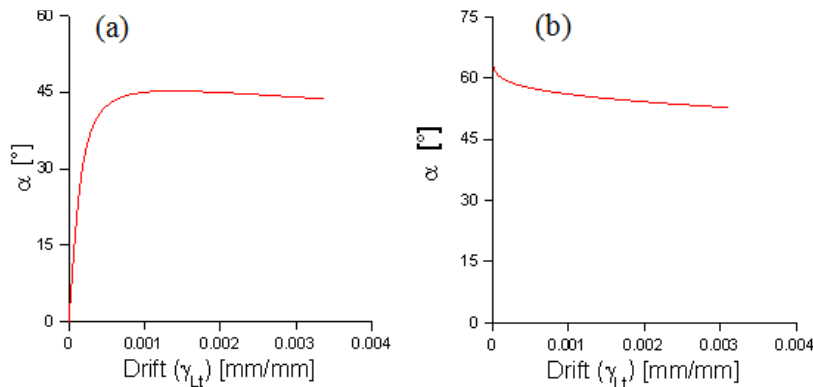

Fig. 3 Estimated principal direction variation with drift: (a) Wall with axial load (T-5; Orakcal *et al*. 2009), and (b) wall without axial load (G-8; Galletly 1952)

it tends to stabilize (the angle is measured between the vertical and the principal compressive direction, then the smaller the value of α, the more vertical becomes the compressive principal strain). This is consistent with the physical response of the wall panel, since before applying lateral loads ($\gamma_{Lt} = 0$) the main compressive direction should be upright ($\alpha = 0$) as the only acting load is the vertical force, N. Once the lateral load appears, the concrete compressive principal strain deviates from the vertical direction due to shear strain, increasing the angle α. In walls without axial load (Fig. 3b), the principal direction varies slightly.

Although this formulation could be used as a simple implementation to obtain the overall load versus displacement response for walls, the use of the calibrated average strain functions (vertical and horizontal) do not guarantee increasing compressive principal strain (ε_d) values for the entire drift range. Even though it is not common, in few cases reduction of compressive strain can be seen for relatively large drift levels. This limitation does not impede analyzing the response for relatively small drift levels, such as initiation of cracking. In the other hand, experimental evidence indicates that once the crack has formed, usually at an early stage, the location of the crack does not rotate showing that principal tensile strain direction remains almost in a fixed angle. Thus, the concept of fixed-crack or fixed-angle approach is investigated.

2.6 Fixed-angle (FA) model

A fixed-angle model assumes that the principal strain (and stress in most cases) direction remains unchanged with loading (e.g., Gupta and Rangan 1998; Kaseem and Elsheikh 2010). For small wall top displacements, cracks have not formed yet, such that a main strut is not defined. Once severe cracking of concrete due to diagonal tension occurs, the strut forms, and its angle begins to stabilize and remains unchanged throughout drift increments.

If the procedure for the rotating-angle model is used to define the direction of the principal strain, a milestone needs to be defined that establishes that the concrete strut has formed in the crack direction. In this case, the strain field is determined with the calibrated expressions for vertical and transverse strains (ε_t and ε_L) and prescribed wall drift values (γ_{Lt}). Upon increments of drift levels, the principal tensile strain increases until the concrete tensile stress is reached $\sigma_r = f_{ct}$. That establishes initiation of cracking (criterion 1); however the strut is not necessarily stabilized (Fig. 3) so that further lateral displacement results in variation of principal direction. Once the strut is considered stable, the strut angle can be defined as the principal strain/stress direction for the fixed-angle model. At relatively large tensile principal strains in concrete, tensile capacity can reduce until zero stress. Considering that at that strain level the compressive strut should have formed, in an average sense, the principal strain direction can be set to the point where half the tensile capacity of concrete has been reduced ($\sigma_r = 0.5f_{ct}$) after cracking, setting the strut direction to a moment between initiation of cracking and zero tensile concrete stress (criterion 2). These two criteria ($\sigma_r = f_{ct}$, consistent with $\varepsilon_r = \varepsilon_{ct}$ and $\sigma_r = 0.5f_{ct}$, consistent with $\varepsilon_r = 0.5(\varepsilon_{ct} + \varepsilon_{ut})$) are used to defined the crack direction for the fixed-angle model, based on the calibrated vertical and horizontal average wall deformations expressions. Sensitivity of the principal direction selection criteria is shown later in the text.

A wide variety of geometric properties (aspect ratio), axial load level, steel reinforcing ratio and material properties were used, based on the experimental database detailed later, in order to determine the crack direction for each model. The drift level was selected for the instant that either

criteria was reached. Given a specific drift level, vertical and horizontal strain values were determined (based on Eq. 17, 19, 21 and 22). Once the crack direction is determined as $\alpha = tan^{-1}\left(-\frac{(\varepsilon_t-\varepsilon_L)}{\gamma_{Lt}} + \sqrt{\left(\frac{\varepsilon_t-\varepsilon_L}{\gamma_{Lt}}\right)^2 + 1}\right)$, the principal tensile strain, based on compatibility equations, is determined as $\varepsilon_r = \frac{\gamma_{Lt}}{2}tan\alpha + \varepsilon_t$ and compared to both possible criteria. Least-square method is used to determine a calibrated expression for the crack direction. Similar parameters as for the vertical and horizontal deformation expressions are used, where the most relevant terms were the ones related to axial load and aspect ratio.

2.6.1 Criterion 1: $\boldsymbol{\sigma_r = f_{ct}}$

The expression is calibrated for cantilever and double-curvature walls, yielding good predictions with the procedure indicated above. Correlation factor (R^2) was 0.98 for the cantilever case, and 0.99 for walls with double curvature. Results are as follows,

$$\underline{\text{Cantilever}} \quad \alpha = 175.2\left(\frac{H_w}{L_w}+5\right)^{-0.605}\left(\frac{N}{f'_c t_w L_w}+1\right)^{-4.6} \tag{23}$$

$$\underline{\text{Double curvature}} \qquad \alpha = 90.6\left(\frac{H_w}{L_w}+5\right)^{-0.25}\left(\frac{N}{f'_c t_w L_w}+1\right)^{-6.65} \tag{24}$$

2.6.2 Criterion 2: $\boldsymbol{\sigma_r = 0.5 f_{ct}}$

Similarly to the previous case, the expression is calibrated for two boundary conditions, yielding good predictions. Correlation factor (R^2) was 0.94 for the cantilever case, and 0.99 for walls with double curvature. Results are as follows,

$$\underline{\text{Cantilever}} \quad \alpha = 143.4\left(\frac{H_w}{L_w}+5\right)^{-0.54}\left(\frac{N}{f'_c t_w L_w}+1\right)^{-1.36} \tag{25}$$

$$\underline{\text{Double curvature}} \qquad \alpha = 102.6\left(\frac{H_w}{L_w}+5\right)^{-0.36}\left(\frac{N}{f'_c t_w L_w}+1\right)^{-2.27} \tag{26}$$

Upon definition of the crack direction (α), the principal strain and stress direction is fixed for the entire analysis. Different drift levels are defined in order to obtain the overall shear load versus shear displacement. Compatibility (Eq. 5-7), material constitutive laws (Eq. 9-16) and vertical equilibrium (Eq. 1) establishes an iterative scheme. The equilibrium equation might be solved using Newton-Rapson. The shear force is determined (Eq. 3, 4), once the vertical equilibrium is satisfied within a tolerance.

3. Model response

3.1 Experimental database

A database that contains 252 specimens was used to validate the proposed model, which are collected from prior studies. This database summarizes the work by Hirosawa (1975) and

Mohammadi-Doostdar and Saatcioglu (2002), and the publications by Massone *et al.* (2009), Hidalgo *et al.* (2002), Yamada *et al.* (1974), Antebi *et al.* (1960), Barda *et al.* (1977), Benjamin and Williams (1957), Cardenas *et al.* (1980), and Galletly (1952). The database includes walls with enlarged boundary elements (68%) as well as rectangular walls (32%), cantilever walls (85%) and walls with double curvature (15%). The vertical boundary steel reinforcement ratio ranges from 0.7% to 11% (of the boundary area). Vertical and horizontal web reinforcement ratio vary between 0% and 3.7%, while the yield stress of all the reinforcing bars are between 209 MPa and 624 MPa. The compressive strength of the concrete varies between 12.4 MPa and 63.4 MPa. The axial load, although applied to few cases, had a maximum ratio of $\frac{N}{f'_c L_w t_w} = 0.27$.

3.2 Strength

In order to determine the shear strength for the entire database, the models (rotating and fixed-angle models) were run for large range of drift levels in order to observe a peak shear force. In the other hand, for the flexural capacity of the wall, a simple flexural model was implemented based on sectional analysis using the same constitutive law for concrete and reinforcing steel, but without the concrete softening ($\zeta = 1$). This was required since most tests indicate a failure mode based on observation, all specifying shear cracking, such that it is not evident whether the flexural capacity (mainly yielding of boundary reinforcement) was reached before excessive shear cracking or crushing, associated with shear failure. Thus, failure type, based on shear and flexural capacity estimates, would be associated to each wall for a specific model.

Table 1 shows the main results for the entire database for the rotating-angle model and the fixed-angle models (both criteria). All rotating-angle and fixed-angle models were run for all specimens. In order to validate the capacity of the model formulation to predict shear capacity, the table rows were divided into specimens with shear and flexural failure. The average ratio between the predicted capacity and the experimental evidence (V_{model}/V_{test}) is shown, together with the standard deviation (SD) and the number of specimens in each failure type group. Regarding the cases associated to shear failure, the rotating-angle model (RA), although simple (non-iterative), underestimates the shear capacity (0.69) with relatively large scatter (0.31). Regarding the fixed-angle models, criterion 1 ($\sigma_r = f_{ct}$, FA1) provides a good strength estimate, but the scatter is similar to the rotating-angle model. Criterion 2 ($\sigma_r = 0.5 f_{ct}$, FA2) shows less scatter (0.26) with a relatively conservative estimate of the shear strength (0.84). In all cases, the number of specimens that is estimated to fail in flexure is around 70 (close to 30% of the database). This shows consistency between the models, especially considering that the average flexural capacity ratio (V_{model}/V_{test}) is close to 1 in all cases. The worse correlation occurs for criterion 1 of the fixed-angle models, where the scatter is larger than in the other two cases, with almost 10 more specimens within this category. This suggests that these specimens are wrongly labeled as flexural failure. All these indicates that criterion 2 of the fixed-angle models presents a good combination of accuracy and small dispersion of data (note that the 0.3 standard deviation of criterion 1 covers 175 specimens, whereas it reduces to 0.26 for criterion 2 for even more specimens - 183).

The inaccuracy of the RA model does not imply that general models with this consideration are incapable of predicting the shear response, but the inconvenience of this specific model lays in the fact that the model is mainly based on strain calibration (vertical and horizontal) and compatibility, using only equilibrium in order to determine the shear strength. In the other hand, the importance

Table 1 Wall shear strength predictions

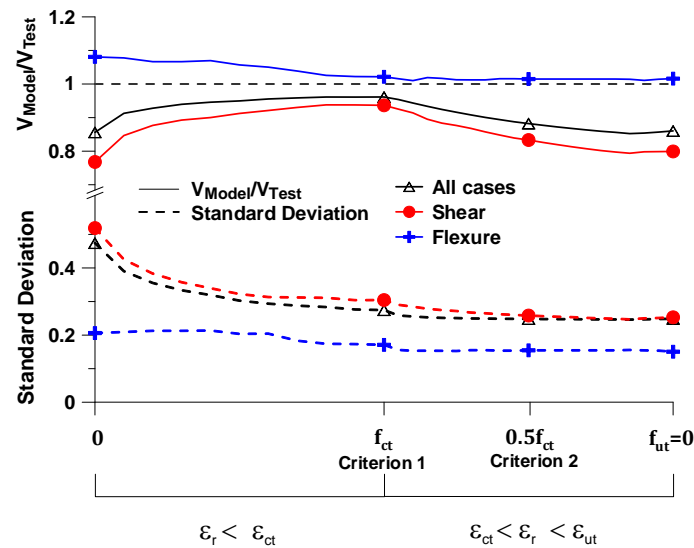| Model	Failure	V_{model}/V_{test}	SD	N° specimens
Rotating angle	All cases	0.77	0.31	252
	shear	0.69	0.31	186
	Flexure	1.0	0.14	66
Fixed angle (Criterion 1)	All cases	0.97	0.27	252
	Shear	0.95	0.30	175
	Flexure	1.03	0.18	77
Fixed angle (Criterion 2)	All cases	0.89	0.24	252
	Shear	0.84	0.26	183
	Flexure	1.02	0.15	69

Fig. 4 Sensitivity of average strength ratio (V_{model}/V_{test}) and standard deviation to criteria selection for the fixed-angle model

of this model is its capability of providing a reasonable estimate of the principal strain direction, α, since strain and compatibility are well captured, which is used for the fixed-angle models.

Regarding the criteria selection for the fixed-angle models, Fig. 4 shows the predicted capacity to experimental ratio (V_{model}/V_{test}) or average strength ratio and standard deviation for cases where the crack formation or the principal angle direction is set for different levels of tensile strain in the direction r (ε_r, x-axis). This analysis required a prescribed value of α for each specimen within the experimental database, and also for each tensile strain level. Each value of α was determined with the RA model, and once known, the fixed-angle model was run for the entire experimental database in order to obtain the shear strength of each wall test. This provides a comparative analysis between both selected criteria for the fixed-angle model and other potential criteria for the same formulation. As it can be seen in Fig. 4, large scatter for the cases labeled as shear failure is observed if the principal direction is forced before cracking ($\varepsilon_r < \varepsilon_{ct}$). This is because the model

provides lower shear strength and several specimens result labeled as flexural failure, increasing also the average strength ratio for flexural cases. Once the selection of principal direction is set after cracking (starting with criterion 1), an important drop of scatter is observed providing progressively lower scatter, but with a lower average strength ratio. At approximately the location of criterion 2, the standard deviation shows further modest reduction, while still the average strength ratio for all cases is just about 10% below 1.0. This indicates that criterion 2 is a plausible selection that provides low scatter and a reasonable strength prediction. No further analysis is provided here, since an optimum value would be attached to the selected material models.

3.3 Strength – parameter sensitivity

This section studies how the strength predictions are sensitive to different wall parameters such as: aspect ratio, web steel reinforcing ratio, axial load, concrete compressive strength and boundary condition. All plots show the strength ratio between the model estimate and the experimental value (V_{model}/V_{test}) versus each parameter under analysis for all specimens. The data corresponds to the fixed-angle model for criterion 2 ($\sigma_r = 0.5f_{ct}$, FA2). Trend lines are included for all models (rotating-angle (RA) model, fixed-angle model with criterion 1 (FA1) and fixed-angle model with criterion 2).

3.3.1 Aspect ratio, H_w/L_w
According to Fig. 5a, all models present good correlation to the aspect ratio, with average strength ratio variation between 10% and 20%, approximately, for the range of test data. Almost all models have trend lines under the strength ratio of 1.0. As the aspect ratio increases, the behavior is more flexural, which is better captured by the model for flexure, resulting in less scatter and with an average close to 1.0.

3.3.2 Longitudinal web steel strength ratio, $\rho_L f_{yL}$
Fixed-angle models present moderate dependency to the longitudinal web steel strength ratio with variation of about 30% to 40% over the data range, whereas the average strength ratio variation increases to about 100% for the range for the rotating-angle model (Fig. 5b). The rotating-angle model tends to be very conservative for low amount of web reinforcement. The better correlation with the fixed-angle models might be related to the fact that in that model, vertical equilibrium is satisfied in the analysis given an important role to the vertical web reinforcement. In all models, conservatism reduces with the increase of the parameter. Similar overall and trend response is observed for transverse web reinforcement strength ratio given that similar web ratio exists in both directions for most tests in the database.

3.3.3 Concrete strength, f'_c
Fixed-angle models present moderate dependency to the concrete strength with variation of about 30% over the data range, whereas the average strength ratio variation increases to about 60% for the range for the rotating-angle model (Fig. 5c). In all models, conservatism reduces with the increase of the parameter.

3.3.4 Wall cross-section and boundary condition
All models present low dependency to the wall cross-section and boundary condition, with similar values for walls with enlarged end sections and rectangular walls, as well as cantilever

walls compared with double-curvature walls (Fig. 5d). Only the rotating-angle model presents a larger dependency to the boundary condition (cantilever versus double curvature). The fixed-angle model with criterion 2 ($\sigma_r = 0.5f_{ct}$) slightly improves the response for rectangular walls compared to walls with enlarged end sections.

3.3.5 Axial load ratio, $N/f'_c t_w L_w$

Fig. 5e shows the dependency of the model to the axial load ratio. The database includes only 15% of specimens with an axial load larger than $0.01f'_c t_w L_w$, because there is little experimental information of walls with axial load. The dependency is moderate for most models with variation of about 40% for all cases. However, for the fixed-angle model with criterion 2 ($\sigma_r = 0.5f_{ct}$) the average strength ratio variation is smaller, better capturing the effect of axial load. In this case, two aspects improve the response to the axial load: (1) the vertical equilibrium includes the effect of the axial load and (2) the principal strain/stress direction is set for larger tensile strains than for criterion 1 ($\sigma_r = f_{ct}$), indicating that crack direction tends to be more horizontal (larger α), when axial load is applied, increasing, in general, its contribution to the shear strength. Thus, the selection of crack formation in criterion 2 seems to be consistent with a good prediction of shear strength for walls with axial load.

Shear capacity in squat walls is known to increase with axial load. Considering that there is little experimental data available in the literature where this aspect has been studied as an isolated variable, the test program by Terzioğlu (2011) is reviewed regarding specimens with similar characteristics. Table 2 includes a selection of specimens that are analyzed in this work. Geometric and material properties, as well as the level of axial load and shear capacity (V_{test}) are included in the table. All specimens were short rectangular walls (aspect ratio equal or less than 1) loaded with a point lateral load applied to the top of the wall. The wall specimens were anchored to a strong floor and tested in cantilever with pseudo-static lateral loads applied with increasing cyclic top drift levels. The axial load was maintained constant throughout the tests.

Specimens SW-T1-S2-9 (Test 9), SW-T1-N5-S1-10 (Test 10) and SW-T1-N10-S1-11 (Test 11) were similar, but with variation of axial load. The axial load was 0, $0.05f'_cA_g$ and $0.1f'_cA_g$ for the specimens, respectively. Fig. 6a shows the analytical and experimental shear strength for these three specimens. All models indicate a capacity increase with axial load, however, the rate of increment is better predicted with the fixed-angle model with criteria 2 ($\sigma_r = 0.5f_{ct}$). The rotating-angle model highly overestimates the increment of shear capacity with axial load in part associated to an underestimation of the response without axial load (Fig. 6a). The fixed-angle model with criteria 1 ($\sigma_r = f_{ct}$) is almost insensitive to the variation of axial load. Considering that the test data indicates an increase of shear strength with axial load, but with a decreased rate with the highest axial load ($0.1f'_cA_g$), it is interesting to analyze the model response for even higher levels of axial loads. Fig. 6b shows the analytical response of a wall with similar characteristics as Test 9, but with variation of axial load. In this case, the response is normalized by the strength estimate for the case with zero axial load. As it can be seen, at low axial load levels, there is an increment of shear capacity with axial load, whose rate of increment reduces with the level of axial load, at a point (in some cases) where the shear capacity decreases for further axial load increments. This is because most of the compressive capacity of concrete and steel (that controls the peak capacity) is Consumed by the application of a large axial load.
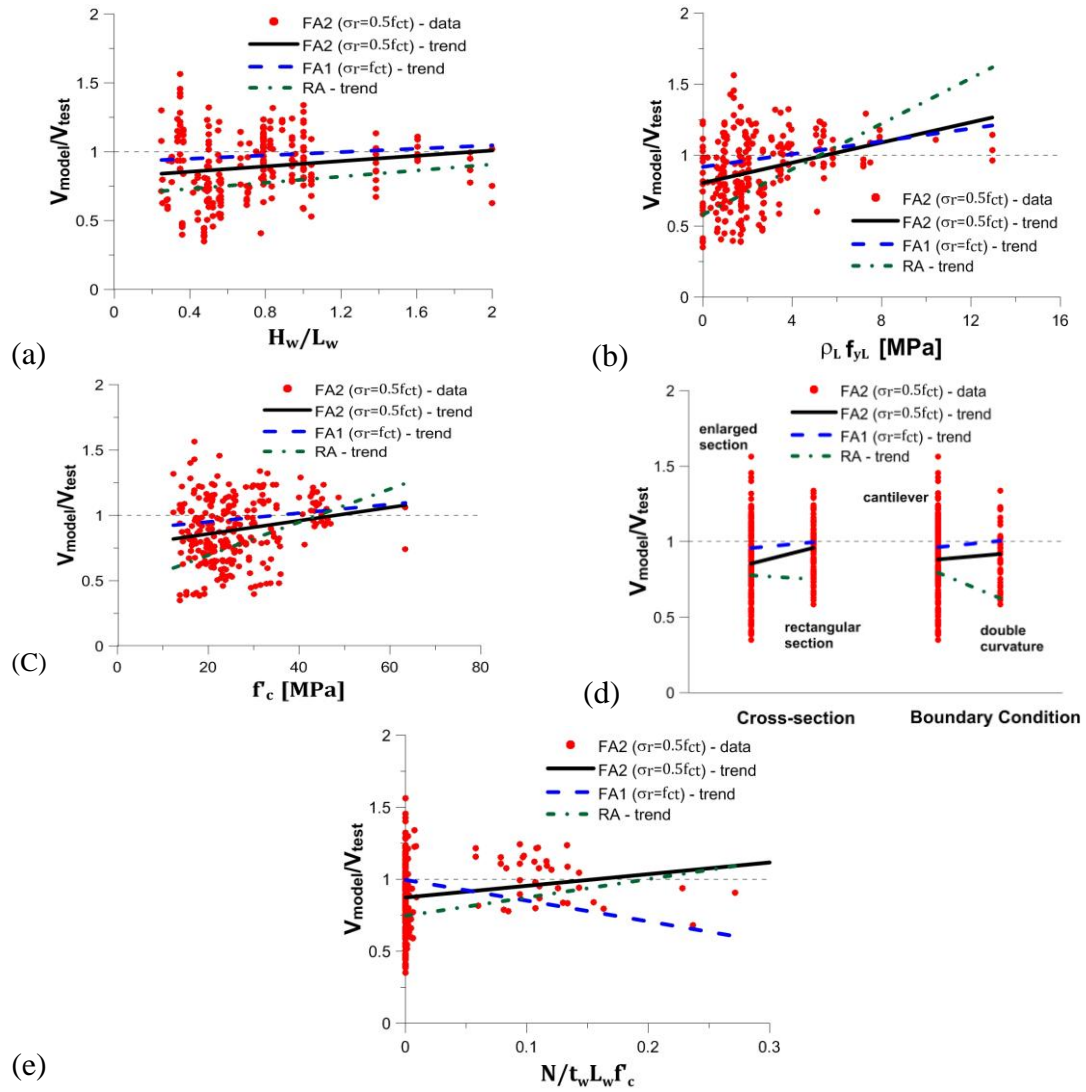
(a)

(b)

(C)

(d)

(e)

Fig. 5 Sensitivity of average strength ratio (V_{model}/V_{test}) to − (a) aspect ratio (H_w/L_w), (b) longitudinal web strength ratio ($\rho_L f_{yL}$), (c) concrete strength (f'_c), (d) wall cross-section and boundary condition and (e) axial load ($N/f'_c t_w L_w$)

Table 2 Wall test characteristics (Terzioğlu 2011)

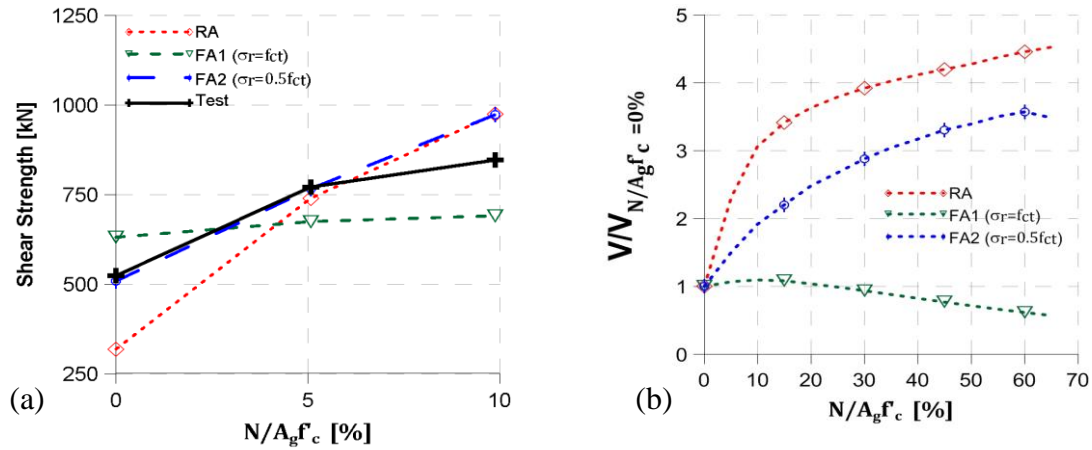| | H_w | L_w | t_w | f'_c | Vertical web | | Horizotal web | | N/f'c | Boundary reinf. | | V test |
					P_t [%]	f_{yt} [%]	ρ_L [%]	F_{yt} [%]	A_g [%]	ρ_b [%]	fy_b [MPa]	[kN]
SW-T2-S1-1	75	150	12	19.3	0.68	481	0.68	481	0	5.15	440	766
SW-T6-S1-8	150	150	12	22.6	0.68	584	0.68	584	0	9.75	528	706
SW-T1-S2-9	75	150	12	24.0	0.34	584	0.34	584	0	5.15	473	524
SW-T1-N5-S1-10	75	150	12	26.3	0.34	584	0.34	584	5	5.15	473	796
SW-T1-N10-S1-11	75	150	12	27.0	0.34	584	0.34	584	10	5.15	473	846

Fig. 6 Shear strength for different axial load levels - (a) absolute strength (predictions and tests) and (b) normalized strength for broad range of axial load (predictions)

3.4 Overall load versus displacement response

As mentioned previously, this type of model allows not only obtaining the shear capacity, but also the overall shear load versus shear displacement response of the wall. This characteristic is suited for pushover analysis of existing or new structures, where commonly the flexural response is captured by a fiber model and the shear response, usually modelled independently from flexure can be captured with the proposed model.

One of the relevant aspects of the overall response is the ability to provide insight into the limit states, especially knowing when collapse or capacity degradation could be observed. In order to capture degradation in the proposed model, the material constitutive laws require cyclic formulations allowing unloading in some of the components, when others are degrading its capacity. A simple unloading branch is set for concrete and steel with stiffness consistent with the material elastic modulus, because just initiation of degradation is required for a pushover (monotonically increasing displacement) analysis.

Three specimens are compared (Fig. 7) for the analysis: (a) SW-T2-S1-1 (Test 1), (b) SW-T6-S1-8 (Test 8) and (c) SW-T1-N5-S1-10 (Test 10) from the test program by Terzioğlu (2011). Since the model is implemented for monotonic loading, the load versus displacement envelop is used as the experimental response. In order to monitor the shear displacement from tests, internal and external sensors were used. Internal diagonal displacement sensors were used to determine shear deformations of the wall. Those sensors were placed within the wall section, such that any sliding between the wall and the pedestal (foundation) was not incorporated. Additional sensors were place in most specimens in order to monitor sliding at the wall-pedestal interface. External diagonal sensors were placed reaching a point in the pedestal, outside the wall. Such instrumentation incorporated the shear within the wall, as well as the sliding shear in the interface (wall-pedestal), which was small for these specimens. Specimen SW-T2-S1-1 was monitored with internal diagonal sensors, whereas for specimens SW-T6-S1-8 and SW-T1-N5-S1-10 the external diagonal sensors were used.
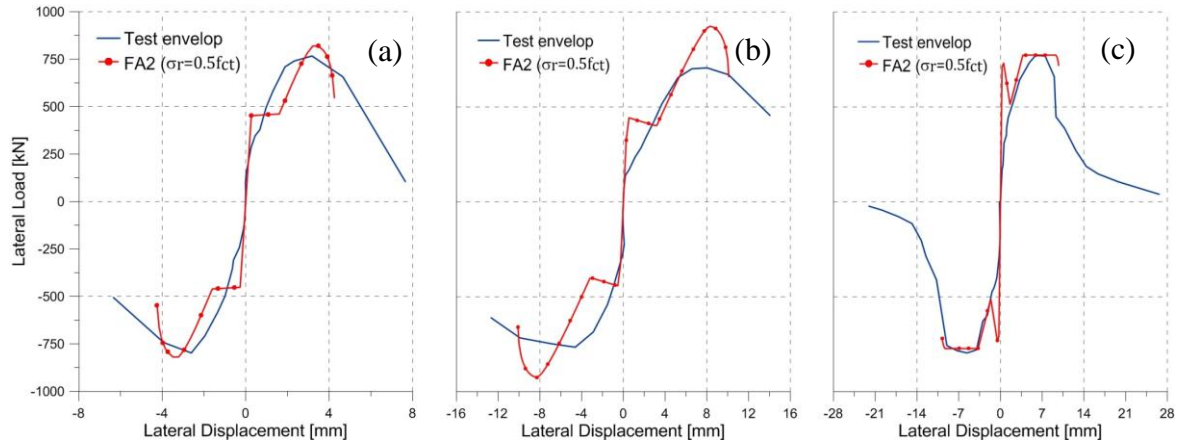
Fig. 7 Model and experimental (Terzioğlu, 2011) shear load versus shear displacement: (a) SW-T2-S1-1, (b) SW-T6-S1-8 and (c) SW-T1-N5-S1-10

Test results are presented for the fixed-angle model with criteria 2 ($\sigma_r = 0.5 f_{ct}$) in Fig. 7, as well as the experimental envelop response. The analytical prediction of the initial stiffness is similar to the experimental values for all cases. The capacity, as expected from the previous analysis, is also similar for all cases even when axial load is applied, however, specimen SW-T6-S1-8 shows less capacity than predicted. That might be associated to the aspect ratio (taller than the other specimens), or a test anomaly since most material parameters present higher capacity or steel quantity. Other aspect of the behavior is the post-cracking response, which is much softer in the experimental program compared to the model. More refined material properties (rather than a simple elasto-plastic steel response, bi-linear tensile response of concrete in tension and almost parabolic constitutive law for concrete in compression) are required to improve the accuracy for post-cracking response. Peak strength at cracking is also higher in the model; probably due to the fact that just a single element is used, impeding an early cracking in the most stressed zones. Softening of the tensile strength of concrete could prevent such difference. Initiation of degradation is also similar in all cases. If we define initiation of degradation as the point where the peak capacity is reduced by 10%, the ratio between the estimated lateral displacement and the experimental data at such point yields values of 0.95, 0.9 and 1.06 for specimens SW-T2-S1-1, SW-T6-S1-8 and SW-T1-N5-S1-10, respectively. All these specimens failed due to diagonal compression, with diagonal cracks forming a series of inclined struts that presented concrete crushing after reaching the peak shear strength. The ability of the model for predicting the point of strength degradation helps defining limit states for pushover analysis.

4. Summary and conclusions

In this work, simple rotating-angle and fixed-angle models capable of predicting the shear load versus shear displacement response of reinforced concrete walls under lateral and axial loads are presented. The models use a wall panel formulation, as seen in previous researches, based on average stress and strain fields for a single reinforced concrete wall panel, with common assumptions such as coincident directions between the principal strain and stress concrete fields,

and perfect adherence between concrete and steel. Concrete response is incorporated in the two principal directions with uniaxial material constitutive laws in tension and compression, including softening of concrete in compression. Web steel reinforcement is represented with an elasto-plastic uniaxial model.

The rotating-angle model uses a formulation where the principal direction (crack inclination) moves or rotates at different drift levels. For each drift level the shear lateral force is calculated using compatibility and material constitutive laws. The strain field is completed by using calibrated expressions for the vertical and horizontal (expansion) average normal strains. Such definition generates a principal direction that rotates with drift levels. Equilibrium is used to determine the shear lateral force at each drift level, without the need of an iterative procedure. Although simple, after relatively large drift levels, the principal compressive strain might present reduction, resulting in a conservative estimate of the shear strength capacity with important scatter. Its accuracy does not invalidate most rotating-angle models, since this one does not apply equilibrium in the vertical direction, but makes it suitable for estimation of principal strain/stress direction, since compatibility and calibrated expressions for vertical and horizontal normal strains are its strength.

The rotating-angle model is used to define the bases for the fixed-angle models. In this case, the principal direction is fixed, trying to represent the physical observation where after diagonal cracking of a wall panel, the principal tensile strain tends to grow orthogonal to the crack direction, maintaining the direction of the principal strain. The crack direction is defined for two alternative models or criteria: (1) at the initiation of cracking ($\sigma_r = f_{ct}$), and (2) once the crack direction is stable and further cracking is observed ($\sigma_r = 0.5 f_{ct}$, post-peak). Sensitivity analysis to the tensile strain that defines the crack direction indicates that criterion 2 presents low scatter for a reasonable average strength prediction. The direction of the crack is defined with the procedure used for the rotating-angle model and calibrated for different wall geometric and material parameters. Upon definition of the crack direction, it is used in junction with the vertical equilibrium equation, which requires solving a non-linear equation for each drift level. The strength predictions for the fixed-angle models (peak capacity) were compared to a database of 252 wall specimens collected from the literature. The ratio between the estimated strength by the models and the experimental strength was 0.97 and 0.89 for criteria (1) and (2), respectively. Close to 30% of the tests were predicted to fail in flexure by a sectional analysis. Good strength estimates of the flexural capacity and low scatter indicates that the method correctly distinguishes between strength controlled by flexure and shear. The shear strength estimates present also low scatter compared to the experimental estimates. Although criterion (1) presents a better average strength ratio estimate the larger scatter indicates that it is less accurate.

Sensitivity analyses of the average strength ratio are performed with all models for different wall parameters (aspect ratio, concrete strength, web steel strength ratio, axial load, web cross-section and boundary condition). In general, the rotating-angle model presents large dependency to most wall parameters indicating that the influence of such parameters in the model are not well predicted. Both fixed-angle models present relatively low dependency of wall parameters to the average strength ratio indicating that the model correctly represents the physical wall behavior. The main difference between both fixed-angle models relates to the axial load. Criterion (2) ($\sigma_r = 0.5 f_{ct}$), presents a better prediction of the shear capacity for walls with axial load. Comparison with test data from a specific experimental program indicates that the shear capacity increases with axial load, which is also well captured by the fixed-angle model with criteria (2). Criteria (1) ($\sigma_r = f_{ct}$) is less dependent to axial load than the experimental evidence.

Finally, the fixed-angle model with criteria (2) ($\sigma_r = 0.5 f_{ct}$) overall shear lateral load versus

shear displacement was compared with the experimental response of tests failing in diagonal compression. The general response is well predicted by the model in particular initiation of strength degradation (10% of capacity reduction), which makes it a desirable model for pushover analysis.

Acknowledgments

References

Antebi, J., Utku, S. and Hansen, R.J. (1960), "The response of shear walls to dynamic loads", Cambridge: Department of Civil and Sanitary Eng., Massachusetts Institute of Technology.

Barda, F., Hanson, J.M. and Corley, W.G. (1977), "Shear strength of low-rise walls with boundary elements", *ACI special publication*—Reinforced concrete structures in seismic zones , SP-**53**, 149-202.

Benjamin, J.R. and Williams, H.A. (1957), "The behavior of one-story reinforced concrete shear walls", *J Struct. Div, ASCE*, **83**(3), 1-49.

Cardenas, A.E., Russell, H.G. and Corley, W.G. (1980), "Strength of low-rise structural walls", *ACI special publication*—Reinforced concrete structures subject to wind and earthquake forces, SP-**63**, 221-421.

Galletly, G.D. (1952), "Behavior of reinforced concrete shear walls under static load", Cambridge: Department of Civil and Sanitary Eng., Massachusetts Institute of Technology.

Gupta, A. and Rangan, B.V. (1998), "High-strength concrete structural walls", *ACI Struct. J.*, **95**(2), 194-205.

Hidalgo, P.A., Ledezma, C.A. and Jordan, R.M. (2002), "Seismic behavior of squat reinforced concrete shear walls", *Earthq. Spectra*, **18**(2), 287-308.

Hirosawa, M. (1975), "Past experimental results on reinforced concrete shear walls and their analysis" (in Japanese), Kenchiku Kenkyu Shiryo. No. 6. Tokyo: Building Research Institute, Ministry of Construction.

Hsu, T.T.C. and Mo, Y.L. (1985), "Softening of concrete in low-rise shearwalls", *ACI Struct J.*, **82**(6), 883-889.

Hsu, T.T.C. and Mo, Y.L. (2010), "Unified Theory of concrete structures", John Wiley & Sons.

Hwang, S.J., Fang, W.H., Lee, H.J. and Yu, H.W. (2001), "Analytical model for predicting shear strength of Squat Walls", *J. Struct. Eng.*, **127**(1), 43-50.

Kaseem, W. and Elsheikh, A. (2010), "Estimation of shear strength of structural shear walls", *J. Struct. Eng.*, **136**(10), 1215-1224.

Massone, L.M. (2010), "Strength prediction of squat structural walls via calibration of a shear-flexure interaction model", *Eng. Struct.*, **32**(4), 922-932.

Massone, L.M., Orakcal, K. and Wallace, J.W. (2009), "Modeling of squat structural walls controlled by shear", *ACI Struct J.*, **106**(5), 646-655.

Mo, Y.L., Zhong J. and Hsu, T.T.C. (2008), "Seismic simulation of RC wall-type structures", *Eng. Struct.*, **30**(11), 3167-3175.

Mohammadi-Doostdar, H. and Saatcioglu, M. (2002), *Behavior and Design of Earthquake Resistant Low-Rise Shear Walls*, Report OCCERC 02-28, Ottawa Carleton Earthquake Engineering Research Center, Canada: Department of Civil Eng., University of Ottawa.

Orakcal, K., Massone, L.M. and Wallace, J.W. (2009), "Shear strength of lightly reinforced wall piers and spandrels", *ACI Struct J.*, **106**(4), 455-465.

Palermo, D. and Vecchio, F.J. (2002), "Behavior of three-dimensional reinforced concrete shear walls", *ACI Struct J.*, **99**(1), 81-89.

Schlaich, J., Schäfer, K. and Jennewein, M. (1987), "Toward a consistent design of structural concrete", *PCI J.*, **32**(3), 75-150.

Terzioğlu, T. (2011), "Experimental evaluation of the lateral load behavior of squat structural walls", Ms Thesis, Civil Engineering Department, Boğaziçi University.

Vecchio, F. and Collins, M.P. (1986), "The modified compression-field theory for reinforced concrete elements subjected to shear", *ACI Struct J.*, **83**(2), 219-231.

Villar, D. (2010), "Modeling and prediction of shear capacity in squat walls via a strut-and-tie model" (in spanish), Engineering thesis, Civil Engineering Department, University of Chile.

Yamada, M., Kawamura, H. and Katagihara, K. (1974), "Reinforced concrete shear walls without openings; test and analysis", *ACI special publication*—Shear in reinforced concrete, SP-**42**, 539-558.

Zhang, L.-X.B. and Hsu, T.T.C. (1998), "Behavior and analysis of 100 MPa concrete membrane elements", *J. Struct. Eng.*, **124**(1), 24-34.